Chapter 3

Sex Difference in the Mouse BAT Transcriptome Reveals a Role of Progesterone in BAT Function

Kasiphak Kaikaew[1,2,*], Aldo Grefhorst[1,3,*], Jacobie Steenbergen[1], Sigrid M.A. Swagemakers[4], Anke McLuskey[1], Jenny A. Visser[1]

1 Department of Internal Medicine, Erasmus MC, University Medical Center Rotterdam, Rotterdam, the Netherlands
2 Department of Physiology, Faculty of Medicine, Chulalongkorn University, Bangkok, Thailand
3 Department of Experimental Vascular Medicine, Amsterdam University Medical Centers, Location AMC, Amsterdam, the Netherlands
4 Department of Pathology and Clinical Bioinformatics, Erasmus MC, University Medical Center Rotterdam, Rotterdam, the Netherlands
* Shared first authorship

Submitted

3

Abstract

Brown adipose tissue (BAT) is a metabolically active organ that exhibits sex-differential features, i.e., being generally more abundant and active in females than in males. Although sex steroids, particularly estrogens, have been shown to regulate BAT thermogenic function, the underlying molecular mechanisms contributing to sexual dimorphism in basal BAT activity have not been elucidated. Therefore, we assessed the transcriptome of interscapular BAT of male and female C57BL/6J mice by RNA sequencing and identified 295 genes showing ≥2-fold differential expression (adjusted $P<0.05$). *In silico* functional annotation clustering suggested an enrichment of genes encoding proteins involved in cell-cell contact, interaction, and adhesion. Ovariectomy reduced the expression of these genes in female BAT towards a male pattern whereas orchiectomy had marginal effects on the transcriptional pattern, indicating a prominent role of female gonadal hormones in this sex-differential expression pattern. Progesterone was identified as a possible upstream regulator of the sex-differentially expressed genes. Studying direct effects of progesterone *in vitro* in primary adipocytes showed that progesterone significantly altered the transcription of several of the identified genes, likely via the glucocorticoid receptor. Moreover, several genes remained sex-differentially expressed under similar *in vitro* culture conditions, indicating intrinsic regulation by the sex origin of cells. In conclusion, this study reveals a sexually dimorphic transcription profile in murine BAT at general housing conditions and demonstrates a role for progesterone in the regulation of the interscapular BAT transcriptome.

Introduction

A growing number of studies suggest that the prevalence of obesity and obesity-related diseases differs between women and men. Although the global prevalence of obesity is higher in women than in men (1), obese men are more prone to develop obesity-related conditions such as type 2 diabetes mellitus than obese women (2). This sex difference diminishes when women enter menopause, suggesting a prominent role for sex steroids, for instance in controlling adipose tissue function since disturbances in adipose tissue function lead to obesity and its associated metabolic diseases (3,4).

In general, two types of adipose tissue with a distinct physiological function can be recognized. White adipose tissue (WAT) serves as the largest energy-storing organ of the body, while brown adipose tissue (BAT) principally utilizes nutrient substrates for non-shivering thermogenesis, crucial for maintaining body temperature in small mammals and human infants (5). In BAT, thermogenesis is activated by the sympathetic nervous system that secretes norepinephrine (NE) upon stimuli such as cold exposure. Thermogenesis depends on uncoupling proton transport by the unique BAT mitochondrial protein, uncoupling protein 1 (UCP1) (6). BAT also plays a role in maintaining optimal energy balance, as illustrated by the development of obesity in UCP1-ablated mice housed at thermoneutral conditions (7). With the confirmation of the presence of active BAT in adults, BAT has been studied extensively because increasing energy expenditure through BAT activation is considered a potential therapeutic option for obesity (8).

While sex differences in WAT and the role of sex steroids herein have been addressed for many years by numerous excellent studies (9), studies on sex differences in BAT functioning and its role in sex-dependent protection against metabolic diseases is largely lacking, although some studies suggest that sex differences may exist in the presence and activity of BAT (10). It was observed that the prevalence of active BAT was about two-fold higher in women than in men (11). Also in rodents, female rats are reported to have higher relative BAT mass, higher BAT UCP1 protein levels, and greater sizes of mitochondria in BAT (12), Moreover, isolated brown adipocytes of female rats had a greater response to NE than those isolated from male rats (12). Circulating sex steroid concentrations are one of the major differences between males and females of reproductive age and therefore are obvious candidates regulating sex differences in BAT activity. Indeed, the roles of sex steroids in sex-differential energy homeostasis have been demonstrated at many levels (10,13). Especially the effects of estrogens on systemic energy balance and BAT activity have been studied in great detail (14,15). For example, ovariectomy in rodents led to an increase in food intake, weight gain, and lipid accumulation in WATs, but also resulted in

reduced thermogenic activity in BAT (16,17), suggesting a stimulating effect of ovarian hormones on BAT activity. In addition, central or peripheral injection of 17β-estradiol (E2) in ovariectomized mice resulted in induced BAT thermogenesis, showing a role for estrogens in stimulating BAT activation via the sympathetic nervous system (18). In contrast, orchiectomy led to increased *Ucp1* mRNA expression and UCP1-positive staining in BAT coinciding with elevated body temperature, revealing an inhibitory effect of male gonadal hormones on BAT thermogenesis (19). Treatment of cultured brown adipocytes with sex steroids confirmed that E2 facilitates while testosterone inhibits NE-induced lipolysis, an initial step of thermogenesis in BAT (20).

While sex steroids may control BAT thermogenic activity, the underlying molecular mechanisms contributing to the sex dimorphism in BAT function are still not fully elucidated. Therefore, in this study we have performed RNA-sequencing (RNA-seq) on the interscapular BAT of male and female mice to identify sex differences in the BAT transcriptome. Identified sex-differentially expressed genes were functionally clustered using available biological databases. We also performed gonadectomy (GDX) to study the roles of sex steroids on the expression of these identified genes. In addition, a possible upstream regulator of the sex-differentially expressed genes was studied in primary cultures of brown adipocytes isolated from male and female mice and in a brown adipocyte cell line.

Materials and Methods

Animals and housing conditions

All animal experiments were approved by the Animal Ethics Committee at Erasmus MC, Rotterdam, the Netherlands. For transcriptional analysis of BAT, 8-week-old male and female C57BL/6J mice were purchased from Charles River Laboratories (Maastricht, Netherlands). Upon arrival, mice were housed at ~22°C on a 12/12-h dark/light cycle with chow diets and water available *ad libitum*. After one-week acclimation, GDX or sham operation was performed as described previously (21). After the surgery, mice were housed at standard housing conditions for 45 days. After these 45 days, the mice were fasted for 4 h and were sacrificed by cardiac puncture under isoflurane anesthesia. BAT was snap-frozen in liquid nitrogen and stored at −80°C until RNA isolation.

For adipose-derived stromal vascular fraction (SVF) cell culture, male and female C57BL/6J mice were bred in the Erasmus MC animal facility and housed under similar conditions. At 20 weeks old, mice were sacrificed by cardiac puncture under isoflurane anesthesia. BAT was dissected and placed in ice-cold PBS (Gibco, Life Technologies Europe, Bleiswijk, Netherlands) containing 100 U/mL of penicillin, 100 µg/mL of streptomycin, and 0.25 µg/mL of Fungizone (Anti-Anti, Gibco) until SVF isolation.

RNA isolation

Total RNA was isolated from BAT using the TriPure isolation reagent (Roche Diagnostics, Mannheim, Germany) and contaminating genomic DNA was removed by the RQ1 RNase-free DNase (Promega Benelux, Leiden, Netherlands), according to the manufacturers' instructions. RNA was quantified with a NanoDrop 2000 spectrophotometer (Isogen Life Science, Utrecht, Netherlands).

Library preparation, RNA sequencing, and expression analysis

RNA quality was assessed by an Agilent 2100 Bioanalyzer (Agilent Technologies, Amstelveen, Netherlands). A TruSeq RNA Library Prep Kit v2 (Illumina, Eindhoven, Netherlands) was used for library preparation according to the manufacturer's instructions. Paired-end sequencing with 50 base pairs in length was performed using a HiSeq 2000 sequencer (Illumina). Adapter sequences were trimmed with Cutadapt (version 1.16 with Python 3.6.4) (22). The trimmed reads were aligned to the mouse reference genome mm10 by RNA STAR (Galaxy version 2.6.0b-2) (23). The number of reads per annotated gene was counted with featureCounts (Galaxy version 1.6.4) (24) using the genome annotation GRCm38 (release 97). The differential expression profile was analyzed in R with DESeq2 (package version 1.25.11) (25). Genes with very low expression (average read counts <3) were removed and genes with the Benjamini-Hochberg (BH)-adjusted P value <0.05 were considered sex-differentially expressed. The *rlog*-normalized counts of the differentially expressed genes were imported into OmniViz (version 6.1.13.0, Instem Scientific, Staffordshire, UK) and visualized with the OmniViz TreeScape (heat maps including dendrograms of the hierarchical clustering).

Enrichment and pathway analysis

Genes with a sex-differential expression ≥2-fold difference were uploaded in DAVID (Bioinformatics Resources, version 6.8; https://david.ncifcrf.gov/) (26). A default DAVID functional annotation (threshold count 2 and EASE 0.1) was performed for Gene Ontology (GO). Subsequently, default DAVID functional annotation tools (e.g. UniProtKB keywords, GO terms, KEGG Pathway, and BioCarta) were selected for functional annotation clustering with a default medium classification stringency (kappa similarity term overlap 3 and threshold 0.5; multiple linkage threshold 0.5; and EASE 0.1).

Next, the ≥2 folds differentially expressed genes together with their $\log_2$-transformed fold differences (female relative to male) were uploaded in Ingenuity Pathway Analysis (IPA, version 49309495; QIAGEN Inc., https://www.qiagenbioinformatics.com/products/ingenuity-pathway-analysis) (27) for expression

analysis using Ingenuity Knowledge Base (genes only) with a default setting (direct and indirect relationships; only experimentally observed confidence) to analyze the functional upstream regulators.

Isolation of SVF cells, cell culture, and *in vitro* hormonal treatment

BAT depots from 5–6 mice were pooled, minced in PBS containing 1% BSA (Sigma-Aldrich, Zwijndrecht, Netherlands) and Anti-Anti (Gibco), and centrifuged at 500 g for 6 min. Tissue suspensions were digested in 1 mg/mL collagenase (Sigma-Aldrich), 2.4 U/mL dispase II (Roche Diagnostics), and 0.5 mg/mL trypsin (Gibco) for 30 min at 37°C with gentle agitation. The digested BAT was filtered through a 100-µm mesh and centrifuged at 400 g for 8 min. Pellets were incubated with RBC lysis buffer (eBioscience, Life Technologies Europe) for 5 min, and then centrifuged at 500 g for 8 min. SVF pellets were resuspended in growth medium [DMEM (4.5 g/L glucose with sodium pyruvate and GlutaMAX) containing 10 mM HEPES, 10% fetal bovine serum (FBS), and Anti-Anti (all from Gibco)] and seeded with 200,000 cells/well in 12-wells plates. After a 24-h attachment period, differentiation was initiated by supplementing the growth medium with 4 nM insulin (Sigma-Aldrich), 1 µM rosiglitazone (Enzo Life Sciences, Brussels, Belgium), and 25 µg/mL L-ascorbic acid (Sigma-Aldrich). This differentiation medium was refreshed every 2–3 days for 13 days. For the female brown preadipocyte cell line T37i [(28); a gift provided by Dr. M. Lombès, Inserm U1185, France], cells were maintained and differentiated for 9 days as described previously (29).

Before progesterone stimulation, fully differentiated BAT SVF or T37i cells were steroid-starved for 3 h in starvation medium [original serum-free medium containing 0.2% dextran-coated charcoal-treated FBS (DCC-FBS), prepared as previously described (29)] after which the cells were pretreated for 60 min with 5 or 500 nM of RU486 (Sigma-Aldrich) or EtOH vehicle. Subsequently, cells were treated for 24 h with the indicated concentrations of progesterone (Steraloids, Newport, RI) or EtOH vehicle supplemented to the starvation medium.

To study the effect of progesterone on differentiation of T37i cells, cells were treated with the indicated concentrations of progesterone or EtOH vehicle supplemented to steroid-deprived T37i differentiation medium (similar to the normal T37i differentiation medium, except replacing 10% FBS with 9% DCC-FBS and 1% FBS). For NE stimulation on differentiated T37i cells, cells were starved for 3 h in 0.2% DCC-FCS starvation medium and subsequently stimulated for 24 h with 1 µM NE (Sigma-Aldrich) or HCl vehicle in the starvation medium.

Glycerol measurement

Cultured media of the NE-stimulated T37i cells were collected, centrifuged for 10 min to remove debris, and used for determination of glycerol concentrations using the glycerol reagent set (INstruchemie, Delfzijl, Netherlands).

Quantitative PCR

Reverse transcription was performed using the Transcriptor high-fidelity cDNA synthesis kit (Roche Diagnostics). Quantitative PCR (qPCR) was performed using the FastStart Universal SYBR Green Master (Rox) (Roche Diagnostics) with a QuantStudio 7 flex real-time PCR system (Applied Biosystems, Life Technologies, Carlsbad, CA). Gene expression was normalized to the indicated housekeeping genes using the $2^{-\Delta\Delta CT}$ method. Primer sequences of all tested genes are listed in **Table 1**.

Results

BAT transcriptional profile of male and female mice

RNA-seq analysis identified 17,798 transcripts in the interscapular BAT of mice, after filtering out transcripts with very low expression levels. Expression levels of these identified transcripts are visualized by the relative female-to-male fold changes in **Fig. 1A**. A total of 2,038 genes were identified being differentially regulated between the sexes (unadjusted $P<0.05$), but when accounting for a BH correction at FDR of 0.1 only 793 transcripts remained differentially expressed. Applying a more stringent BH-adjusted $P<0.05$, trimmed the number to 596 transcripts (**Fig. 1A** and **1B**). Of these 596 genes, 347 genes (58.2%) showed a female-biased expression and 249 genes (41.8%) showed a male-biased expression (**Fig. 1B**). Further trimming by applying a cut-off of two-fold difference resulted in 295 genes being significantly sex-differentially expressed, of which 242 genes (82.0%) showed higher expression and 53 genes (18.0%) showed lower expression in female BAT than in male BAT (**Fig. 1B**). Hierarchical clustering analysis of the 295 genes illustrates the differences in BAT transcriptional profile between male and female mice (**Fig. 1C**).

Analysis of biological processes of the sex-differentially expressed genes

Of the 295 sex-differentially expressed genes, 291 genes were matched in the DAVID mouse data resources. Top GO annotation terms from enrichment analyses are presented in **Table 2** and top significant functional annotation clusters are presented in **Table 3**. In general, among the leading significant categories and clusters are genes that encode proteins involved in cellular structure and cell-cell contact, interaction, and adhesion.

Table 1 Primer sequences

Gene	Forward (5′→3′)	Reverse (5′→3′)
Adipoq	GCACTGGCAAGTTCTACTGCAA	GTAGGTGAAGAGAACGGCCTTGT
Bax	TGAAGACAGGGGCCTTTTTG	AATTCGCCGGAGACACTCG
Bcl2	GGACTTGAAGTGCCATTGGT	CATCACGATCTCCCGGTTAT
Bmp8b	CAACCACGCCACTATGCAG	CACTCAGCTCAGTAGGCACA
C7	CAACTGCAAGTGGGACTCCTA	CAGCAACTGAACGCCTTCG
Cdh1	AGACTTTGGTGTGGGTCAGG	ATCTGTGGCGATGATGAGAG
Cfd	CTACAAGCGATGGTATGATGTGC	GGACCCAACGAGGCATTCT
Cldn3	AGTGCTTTTCCTGTTGGCGGCTCT	ATCGCGGCGCAGAATAGAGGATCT
Cldn4	CAGTGCAAGATGTACGACTCGAT	TACCACTGAGAGAAGCATCCCC
Cldn7	AGGGTCTGCTCTGGTCCT	GTACGCAGCTTTGCTTTCA
Cxcl13	CATAGATCGGATTCAAGTTACGCC	TCTTGGTCCAGATCACAACTTCA
Epcam	GCGGCTCAGAGAGACTGTG	CCAAGCATTTAGACGCCAGTTT
Esr1	TGGGTCATGAGAGTCCTTTGAA	CCGGGATGGAAACTGAACTTT
Fabp4	GCGAGTAGAATGACAGCTCCTT	CTGTCGTCTGCGGTGATTT
Fkbp5	ATTTGATTGCCGAGATGTG	TCTTCACCAGGGCTTTGTC
Irf4	TGCAAGCTCTTTGACACACA	CAAAGCACAGAGTCACCTGG
Krt5	TCTGCCATCACCCCATCTGT	CCTCCGCCAGAACTGTAGGA
Krt8	CAAGGTGGAACTAGAGTCCCG	CTCGTACTGGGCACGAACTTC
Krt14	CCACCTTTCATCTTCCCAATTCTC	GTGCGGATCTGGCGGTTG
Krt18	CTGGAGGATGGAGAAGATTT	CTTTTATTGGTCCCTCAGTT
Lcn2	ACTTCCGGAGCGATCAGTT	CAGCTCCTTGGTTCTTCCAT
Lep	ACCCCATTCTGAGTTTGTCC	TCCAGGTCATTGGCTATCTG
*Mup**	CAAAACAGAAAAGGCTGGTGA	TTGTGCAAACCTTTCCTTGA
Nr3c1	CCGGGTCCCCAGGTAAAGA	TGTCCGGTAAAATAAGAGGCTTG
Pgr	GGGGTGGAGGTCGTACAAG	GCGAGTAGAATGACAGCTCCTT
Pparg	GAAAGACAACGGACAAATCACC	GGGGGTGATATGTTTGAACTTG
Ppargc1a	CCCTGCCATTGTTAAGACC	TGCTGCTGTTCCTGTTTTC
Ptprf	TGCTCTCGTGATGCTTGGTTT	ATCCACGTAATTCGAGGCTTG
Scnn1b	ACCCGGTGGTTCTCAATTTGT	AAGTTCCGCAAGGTACACACA
Sdc1	TGGAGAACAAGACTTCACCTTTG	CTCCCAGCACTTCCTTCCT
St14	TCATCGCCTACTACTGGTCAGAGT	TGGCGCGATCAACCTCTT
Tsc22d3	CAGCAGCCACTCAAACCAGC	ACCACATCCCCTCCAAGCAG
Ucp1	GGCCTCTACGACTCAGTCCA	TAAGCCGGCTGAGATCTTGT
Wfdc2	AACCAATTACGGACTGTGTGTT	TCGCTCGGTCCATTAGGCT
Actb	AAGGCCAACCGTGAAAAGAT	GTGGTACGACCAGAGGCATAC
B2m	ATCCAAATGCTGAAGAACGG	CAGTCTCAGTGGGGGTGAAT
Hprt	GCAGTACAGCCCCAAAATGG	AACAAAGTCTGGCCTGTATCCAA
Rn18s	GTAACCCGTTGAACCCCATT	CCATCCAATCGGTAGTAGCG

* The primers detect multiple genes of the MUP family due to its high similarity in mRNA sequences.

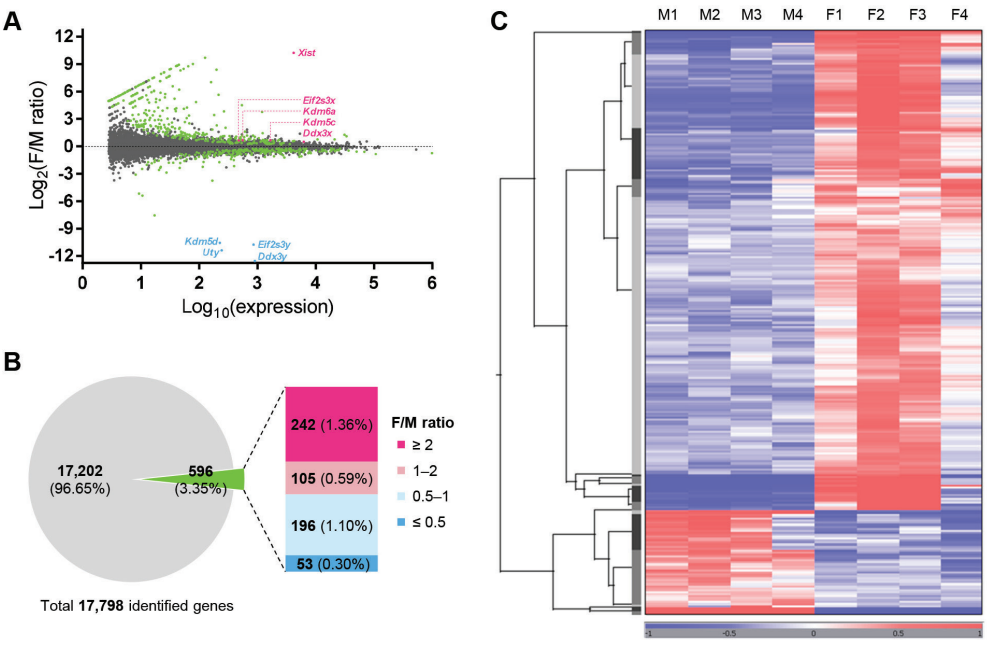

Fig. 1 Sex difference in BAT RNA-seq profile

(A) Scatter plot demonstrating expression levels of all identified genes. Log-transformed average normalized counts of genes in BAT are presented on the X axis and log-transformed fold changes are presented on the Y axis, with positive values indicating female-biased expression and negative values indicating male-biased expression. Blue and pink dots represent known differentially expressed genes and serve as internal controls: blue indicates Y-chromosomal genes, whereas pink indicates X gametologs of the Y-chromosomal genes and the major X inactivation gene, *Xist*. Green dots indicate the significant sex-differentially expressed genes (BH-adjusted $P<0.05$). **(B)** Pie and bar chart demonstrating the number and percentage of identified genes. A two-fold cut-off was applied to select genes with a substantial sex-dependent expression. **(C)** Heat map and dendrogram presenting the expression of the 295 sex-differentially expressed genes (BH-adjusted $P<0.05$ and differential expression ≥2 folds) in BAT of 4 male (M1–M4) and 4 female (F1–F4) mice. Red indicates upregulation and blue indicates downregulation, compared to the geometric mean of the *rlog*-normalized expression levels of each gene, and the color intensity represents the magnitude of the difference.

Table 2 Top GO terms in each annotation category by enrichment analysis in DAVID

GO Term	Count	%	*P* value
Biological process			
Cell adhesion	23	7.90	7.00E−7
Mammary gland alveolus development	5	1.72	1.05E−4
Cellular response to platelet-derived growth factor stimulus	5	1.72	2.30E−4
Sodium ion transport	9	3.09	2.73E−4
Positive regulation of fat cell differentiation	6	2.06	4.95E−4
Canonical Wnt signaling pathway	7	2.41	0.001
Cellular component			
Extracellular exosome	87	29.90	2.89E−16
Extracellular region	60	20.62	8.36E−12
Proteinaceous extracellular matrix	23	7.90	2.02E−10
Extracellular space	48	16.49	1.79E−8
Apicolateral plasma membrane	7	2.41	2.17E−7
Cell junction	29	9.97	2.68E−7
Molecular function			
Structural molecule activity	16	5.50	5.19E−7
Symporter activity	10	3.44	1.63E−5
Cell adhesion molecule binding	8	2.75	3.88E−5
Protein binding	78	26.80	2.43E−4
Scaffold protein binding	6	2.06	6.28E−4
Transcriptional activator activity, RNA polymerase II core promoter proximal region sequence-specific binding	12	4.12	8.79E−4

Count indicates the number of sex-differentially regulated genes in the GO term and % was calculated based on the total of 291 sex-differentially expressed genes uploaded in DAVID. *P* value indicates a modified Fisher exact test, the DAVID enrichment (EASE score) analysis.

Table 3 Top functional annotation clusters by DAVID, presenting only GO terms

Cluster 1	Enrichment score 10.351
GO terms	Extracellular region; Extracellular space
Genes	Acta2, Actg2, Adamts15, Adamts18, Alcam, Ano9, Anxa2, Apln, Aqp5, Areg, Atp4b, Bglap3, Bmp8b, Bnc2, Bsn, Btn1a1, C7, Ccdc3, Ccr3, Cdcp1, Cdh1, Cdh3, Cdh11, Cel, Cfd, Chil1, Clca3a2, Col4a6, Col9a2, Col12a1, Col17a1, Csn3, Ctse, Cxcl13, Cxcl15, Dkkl1, Dmbt1, Dmkn, Dsg2, Epcam, Ephb3, Ezr, Faim2, Fam20c, Fbn2, Fcgbp, Fetub, Fgb, Flrt1, Frem1, Fxyd3, Galnt3, Gcnt4, Ggt1, Gldn, Glt1d1, Gpr156, Gpx3, Hc, Igfals, Il17b, Itgb3, Itih2, Krt8, Krt14, Krt18, Krtdap, Lad1, Lama1, Lamc2, Large2, Lcn2, Lgals7, Ltf, Lvrn, Ly6d, Mfap2, Mfap4, Mfsd2a, Muc15, Mup1*, Myc, Ncan, Nectin4, Nipal2, Npr3, Nt5e, Olfm2, Oxtr, Pdgfd, Phyhip, Piezo2, Plb1, Plet1, Plod2, Plppr3, Prlr, Proc, Prom1, Prom2, Prtn3, Ptk7, Ptn, Ptprf, Ptprn2, R3hdml, S100a9, Scg3, Scnn1b, Sdc1, Serpinb5, Slc1a1, Slc5a1, Slc5a5, Slc5a7, Slc5a8, Slc5a9, Slc6a13, Slc12a2, Slc38a1, Slc44a4, Slco2a1, Slit2, Spint2, Spon1, St14, Sucnr1, Tacstd2, Thsd4, Tlr5, Tmem119, Tmprss2, Tmprss13, Tpbg, Tspan1, Upk3a, Vtcn1, Wfdc2, Wfdc18, Wisp2, Wnt7b
Cluster 2	Enrichment score 3.902
GO terms	Membrane; Plasma membrane
Genes	Abcc8, Alcam, Ano9, Anxa2, Ap1m2, Aqp5, Areg, Atp4b, Atp6v1b1, Basp1, Bnc2, Btn1a1, Cacna1g, Cadps2, Ccr3, Cdcp1, Cdh1, Cdh3, Cdh11, Cldn3, Cldn4, Cldn7, Cldn8, Clic6, Col17a1, Ddx3y, Dmbt1, Dsg2, Dsp, Epcam, Ephb3, Esyt3, Ezr, Faim2, Fer1l4, Fermt1, Flrt1, Fxyd3, Galnt3, Gcnt4, Ggt1, Gldn, Gpr156, Hpd, Irf4, Irs1, Itgb3, Kcng4, Krt5, Krt19, Lamc2, Large2, Lvrn, Ly6d, Marveld3, Mfsd2a, Mmd2, Mrgprg, Mtmr7, Muc15, Ncan, Nectin4, Nipal2, Npr3, Nt5e, Olfm2, Oxtr, Pdgfd, Perp, Pgr, Piezo2, Pkp1, Plb1, Plch2, Plet1, Plod2, Plppr3, Pmepa1, Prlr, Prom1, Prom2, Prtn3, Ptk7, Ptn, Ptprf, Ptprn2, S100a14, S100a9, Scg3, Scnn1b, Sdc1, Slc1a1, Slc5a1, Slc5a5, Slc5a7, Slc5a8, Slc5a9, Slc6a13, Slc12a2, Slc35f3, Slc38a1, Slc44a4, Slco2a1, Slit2, Smim3, Spint2, St14, Sucnr1, Syt14, Tacstd2, Tlr5, Tmem45b, Tmem56, Tmem119, Tmprss2, Tmprss13, Tpbg, Tspan1, Tusc5, Upk3a, Vtcn1, Wisp2, Wnt7b, Wwc1, 6430571L13Rik
Cluster 3	Enrichment score 3.542
GO terms	Structural molecule activity; Cell periphery; Scaffold protein binding; Intermediate filament
Genes	Actg2, Cacna1g, Cdh1, Cgn, Cldn3, Cldn4, Cldn7, Cldn8, Col4a6, Dsp, Ezr, Fgb, Krt5, Krt8, Krt14, Krt15, Krt17, Krt18, Krt19, Lad1, Sprr1a
Cluster 4	Enrichment score 3.295
GO terms	Symporter activity; Sodium ion transport; Transporter activity; Ion transport
Genes	Aqp5, Atp4b, Cacna1g, Clic6, Fxyd3, Kcng4, Lcn2, Ltf, Mfsd2a, Mup1*, Piezo2, Scnn1b, Slc1a1, Slc5a1, Slc5a5, Slc5a7, Slc5a8, Slc5a9, Slc6a13, Slc12a2, Slc38a1, Slco2a1
Cluster 5	Enrichment score 3.022
GO terms	Apicolateral plasma membrane; Bicellular tight junction; Calcium-independent cell-cell adhesion via plasma membrane cell-adhesion molecules
Genes	Alcam, Cdh1, Cdh3, Cgn, Cldn3, Cldn4, Cldn7, Cldn8, Epcam, Ezr, Krt8, Krt19, Mapk13, Marveld3, Perp, Pof1b, Ptprf, Rasgrf1, Sdc1, Vtcn1

* Mup1 was entered in DAVID as a representative for Mup22 due to its highly similar protein sequences (https://www.uniprot.org/uniprot/Q4FZE8).

Validation of the sex-differentially expressed genes by qPCR and influences of GDX

We selected a subset of genes, corresponding to the first five significant functional annotation clusters that showed a high sex-differential expression level in BAT according to the RNA-seq analysis. The summary of their known biological function is reported in the supplementary table, available in an online repository (30). Since sex steroids have been implicated to contribute to sex differences in BAT function (15), expression of these selected genes was validated in BAT of both sham-operated and gonadectomized mice by qPCR (**Fig. 2**). This analysis confirmed that sham-operated female mice had higher BAT mRNA expression of cell adhesion and structural molecules, e.g. epithelial cadherin (E-cadherin), claudins, epithelial cell adhesion molecule (EpCAM), keratins, and syndecan 1 than sham-operated male mice (**Fig. 2**). Removal of female sex steroids by GDX significantly reduced the expression of these genes, but GDX in males only had marginal effects. Hence, female gonadal factors are likely important regulators of the expression of cell adhesion and structural molecules in interscapular BAT of mice.

Analysis of possible upstream regulators and its regulated genes

Next, we investigated possible regulators of the sex-differentially expressed genes in BAT by upstream regulator analysis in IPA. Top significant upstream regulators are presented in **Table 4**. In the gene, RNA, and protein category (**Table 4**), erb-b2 receptor tyrosine kinase 2 (ErbB2, also known as human epidermal growth factor receptor 2 [HER2]) and transforming growth factor (TGF)-β1 were identified as the top upstream regulators. The predicted state of ErbB2 on sex-differential (female over male) BAT transcriptome was an activation (Z=3.58), as well as that of TGF-β1, except that the prediction was less confident (Z=1.48). Interestingly, another top identified upstream regulator was the estrogen receptor which is in agreement with the finding that E2 was the top upstream regulator in the endogenous chemical category (P=2.45×10^{-11}; **Table 4**). The activation state of E2 on sex-differential (female over male) BAT transcriptome was predicted as an activation (Z=3.88). Another female sex steroid, progesterone, was predicted as the second upstream regulator in the endogenous chemical category (P=1.78×10^{-7}) and its activation state was possibly an activation (Z=1.35), albeit with less confidence than E2. Tretinoin (also known as all-trans retinoic acid) and dihydrotestosterone (DHT) were identified as additional upstream regulators (P=3.02×10^{-7} and P=6.20×10^{-5} respectively), but their activation states were uncertain.

The identification of E2 and estrogen receptor as upstream regulators is in line with previous studies implicating a role for E2 in the activation of BAT (15). However, involvement of progesterone in BAT function is less clear. In this study, we decided to further investigate effects of progesterone on BAT.

Genes	RNA-seq F/M ratio, mean (95% CI)	qPCR relative expression level, mean±SEM				
		Male sham	Female sham	Male GDX	Female GDX	Sig.
Epcam	520.3 (88.4–3060.7)	1.00±0.37	698.2±247.9 $	0.27±0.07	19.00±11.01 $,#	×,S,G
Pgr†	439.9 (43.7–4433.0)	1.00±0.49	1.80±0.38	0.42±0.25	0.15±0.08 #	G
Wfdc2†	343.6 (69.3–1703.1)	1.00±0.18	155.8±15.9 $	0.96±0.08	6.91±2.03 $,#	×,S,G
Krt8	332.5 (68.3–1619.0)	1.00±0.22	2616.0±588.2 $	0.94±0.12	63.07±46.06 $,#	×,S,G
Cldn4†	315.0 (49.8–1992.2)	1.00±0.07	1486.6±387.7 $	1.22±0.10	56.81±7.47 $,#	×,S,G
Krt14	243.6 (45.4–1308.0)	1.00±0.41	172.8±48.8 $	0.39±0.06	5.55±3.08 ($),#	×,S,G
Krt5†	197.8 (38.5–1014.7)	1.00±0.19	6.35±1.26 $	1.04±0.26	1.26±0.33 #	×,S,G
Krt18	129.5 (37.0–453.2)	1.00±0.28	788.6±143.9 $	0.34±0.08 (#)	20.91±7.82 $,#	×,S,G
Mup22	38.31 (7.08–207.4)	1.00±0.20	17.17±6.73 $	0.92±0.29	1.46±0.65 #	×,S,G
Scnn1b†	25.90 (4.44–151.2)	1.00±0.19	34.53±12.61 $	0.60±0.08	1.99±0.42 #	S,G
Cldn3†	19.18 (7.50–49.06)	1.00±0.21	103.6±33.1 $	1.59±0.49	6.26±1.29 $,#	×,S,G
Bmp8b	18.80 (9.08–38.92)	1.00±0.57	28.46±12.26 $	0.29±0.06	1.71±0.19 $,#	(×),S,G
Cdh1†	17.19 (7.98–37.02)	1.00±0.04	26.86±7.88 $	0.69±0.23	2.12±0.45 $,#	×,S,G
Lcn2†	10.33 (5.75–18.56)	1.00±0.62	4.98±2.14 $	0.77±0.39	0.32±0.13 #	(×),(G)
St14	8.20 (3.88–17.35)	1.00±0.28	11.90±3.05 $	0.67±0.19	2.84±0.65 $,#	S,G
Cldn7	7.33 (2.69–19.97)	1.00±0.18	25.20±6.40 $	0.60±0.11	2.95±0.84 $,#	×,S,G
Irf4	3.08 (2.15–4.41)	1.00±0.29	3.23±0.41 $	2.34±0.56 (#)	1.11±0.30 #	×
Ptprf	2.53 (1.63–3.94)	1.00±0.15	1.97±0.50	0.79±0.12	0.64±0.06 #	G
Cfd†	2.41 (1.74–3.33)	1.00±0.30	5.17±1.02 $	1.78±0.25	1.05±0.33 #	×,(S)
Sdc1	2.36 (1.70–3.26)	1.00±0.11	1.77±0.31 $	0.96±0.09	0.75±0.14 #	×,G
Cxcl13	0.14 (0.08–0.25)	1.00±0.29	0.39±0.09	2.95±1.32	0.22±0.10 $	(×),S
C7	0.07 (0.06–0.10)	1.00±0.31	0.08±0.00 $	1.12±0.46	0.12±0.03 $	S

Relative expression

2^{9}
2^{6}
2^{3}
2^{0}
2^{-3}
2^{-6}
2^{-9}

Fig. 2 Validation of gene expression by qPCR and influences of sex and GDX on sex-differential expression in BAT

The relative female/male (F/M) expression ratios by RNA-seq are shown in descending order in the left column. DESeq2-estimated $\log_2$-transformed fold changes (lfc) and the standard error of the lfc (lfcSE) were used to calculate the F/M ratio by 2^{lfc} and the 95% confidence interval by $2^{lfc-1.96(lfcSE)}$ and $2^{lfc+1.96(lfcSE)}$. † indicates genes that the Ingenuity database identified as progesterone-regulated molecules. The other columns present relative expression levels measured by qPCR. Expression levels were normalized to *B2m* and *Rn18s* and are shown relative to the sham-operated male mice. The Sig. column lists significant effects (P<0.05) analyzed from the log-transformed expression levels by two-way ANOVA: G for gonadal status (sham or GDX), S for sex, and × for an interaction between G and S. $ indicates a significant sex difference between mice with the same gonadal status and # indicates a significant effect of gonadal status within the same sex, by *post hoc* test (P<0.05). Symbol in parentheses indicates a tendency to significance (P<0.10). Color demonstrates $\log_2$-transformed relative expression levels. Abbreviation of operation: GDX, gonadectomy.

Table 4 Upstream regulator analysis of sex-differential expression in BAT by IPA

Upstream Regulator	Molecule Type	Activation *Z* score	*P* value of overlap
Genes, RNAs, and Proteins			
ERBB2	kinase	3.58	1.16E−15
estrogen receptor	group	1.43	2.43E−15
TGFB1	growth factor	1.48	7.14E−13
CAV1	transmembrane receptor		1.53E−12
KLF4	transcription regulator	3.55	1.51E−11
CEBPA	transcription regulator	0.22	5.91E−11
TNF	cytokine	1.15	4.68E−10
CCN5	growth factor	1.27	6.00E−10
SOX2	transcription regulator	0.58	9.36E−10
EGF	growth factor	1.23	1.07E−09
Endogenous Chemicals			
17β-estradiol	endogenous chemical	3.88	2.45E−11
progesterone	endogenous chemical	1.35	1.78E−7
tretinoin	endogenous chemical	−0.10	3.02E−7
dihydrotestosterone	endogenous chemical	0.53	6.20E−5

Activation *Z* score identifies upstream regulators that can explain observed gene expression fold changes in the dataset and predicts the activation state of the possible upstream regulators based on the Ingenuity Knowledge Base. *Z*>2 indicates a significant prediction of an activated state whereas *Z*<−2 indicates a significant prediction of an inhibited state. *P* value of overlap indicates enrichment of the database-known regulated genes in the dataset.

Effects of progesterone on the RNA-seq–identified sex-differentially expressed genes in SVF-differentiated brown adipocytes

Direct effects of progesterone on the gene transcription of the validated sex-differentially expressed genes reported in **Fig. 2** was assessed in SVF-differentiated primary brown adipocytes. Ingenuity database identified a total of 25 genes as progesterone-regulated molecules in our dataset, of which 9 genes (*Cdh1*, *Cfd*, *Cldn3*, *Cldn4*, *Krt5*, *Lcn2*, *Pgr*, *Scnn1b*, and *Wfdc2)* were among the qPCR-validated genes in BAT. We first determined whether these 9 IPA-identified progesterone-regulated genes were detectable in male and female SVF-differentiated brown adipocytes by qPCR. We could only detect mRNA expression of *Cfd*, *Lcn2*, and *Pgr* (**Fig. 3A**), of which the expression levels at basal conditions in primary brown adipocytes confirmed the higher expression levels in female than in male BAT. Progesterone stimulation for 24 hours revealed that progesterone dose-dependently reduced *Cfd* mRNA expression in differentiated

SVFs of both sexes (**Fig. 3B**), while it induced *Lcn2* (**Fig. 3C**) but reduced *Pgr* (**Fig. 3D**) mRNA expression more prominently in female adipocytes than in male adipocytes.

Apart from *Pgr*, which encodes the nuclear progesterone receptor (PR) and is a known progesterone-regulated gene, we also investigated the mRNA expression levels of other nuclear receptors to determine whether they may underlie the progesterone effects. Interestingly, progesterone dose-dependently reduced *Nr3c1* [encoding the glucocorticoid receptor (GR)] mRNA expression in adipocytes of both sexes (**Fig. 3E**). Moreover, mRNA expression of a GR-target gene *Tsc22d3* [also known as glucocorticoid-induced leucine zipper (*Gilz*)] was dose-dependently upregulated by progesterone treatment in adipocytes of both sexes (**Fig. 3F**), implicating involvement of GR signaling in the progesterone effects in these SVFs.

As RU486 is a PR- and GR-antagonist with a more PR-specific competitive antagonism at low concentrations (i.e. 5 nM) and a dual PR- and GR-antagonism at high concentrations (i.e. 500 nM) (31), we co-administrated progesterone with 5 or 500 nM of RU486 to study the contribution of PR and GR in the observed progesterone effects. Noticeably, the progesterone-induced upregulation of *Tsc22d3* mRNA expression remained unaffected upon 5 nM of RU486 co-administration, but was blocked in the presence of 500 nM of RU486 (**Fig. 3F**), confirming specificity of the selected RU486 doses. Similarly, we observed that progesterone influences on *Cfd*, *Lcn2*, and *Pgr* (**Fig. 3B–3D**) mRNA expression levels were marginally affected at 5 nM of RU486, but were completely blunted with 500 nM of RU486 cotreatment, suggesting GR-mediated responses of progesterone on these genes.

Next, we determined whether progesterone could affect the expression of the 13 qPCR-validated sex-differentially expressed genes not present in the IPA database of progesterone-regulated molecules (**Fig. 2**). By qPCR, only the mRNA expression of *C7*, *Ptprf*, *Scd1*, and *Krt14* was detectable in SVF-differentiated primary brown adipocytes (**Fig. 3G**). Unlike the expression pattern observed in the interscapular BAT, we found that mRNA expression levels of *C7* were higher in female- than in male-derived adipocytes and progesterone treatment of differentiated SVFs stimulated *C7* mRNA expression in adipocytes of both sexes (**Fig. 3H**). This stimulatory effect was abolished only by the 500 nM of RU486 but not by the 5 nM of RU486 cotreatment. Progesterone marginally inhibited *Ptprf* mRNA expression only in male-derived adipocytes (**Fig. 3I**) but did not affect *Sdc1* (**Fig. 3J**) and *Krt14* (data not shown) mRNA expression in cells of either sex. Of note, the finding that mRNA expression of only 7 out of 22 qPCR-validated sex-differentially expressed genes in the interscapular BAT were detectable in primary brown adipocytes (**Fig. 3A** and **3G**) suggests that these other 15 genes may be expressed by other cell types in the BAT depot.

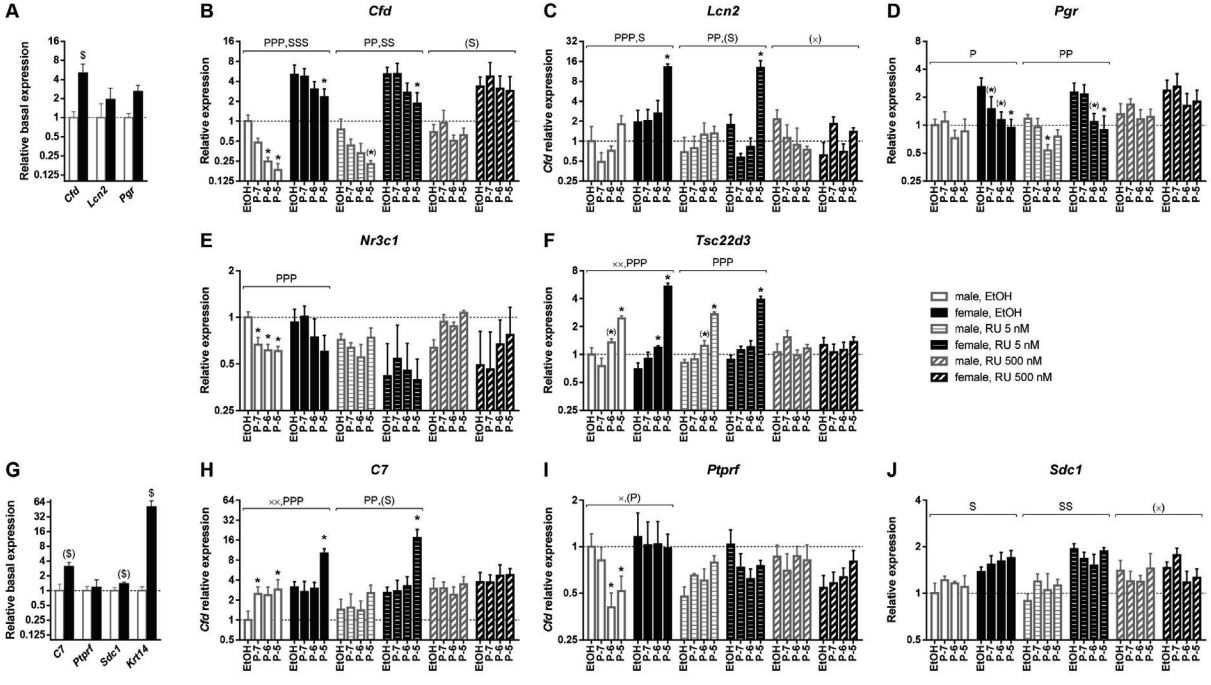

Fig. 3 Effects of progesterone on the RNA-seq–identified sex-differentially expressed genes in SVF-differentiated brown adipocytes

SVF-derived primary cultures of brown adipocytes from male and female BAT were stimulated with progesterone at indicated concentrations: P-7 (10^{-7} M), P-6 (10^{-6} M), or P-5 (10^{-5} M), together with RU486 (5 or 500 nM) or EtOH vehicle. Expression levels were normalized to *Actb* and *Hprt*, depicted relative to the level of EtOH-treated male adipocytes, and presented as mean±SEM. Data were log-transformed before statistical analyses. Basal mRNA expression levels of **(A)** the RNA-seq–identified sex-differentially expressed and IPA-identified progesterone-regulated genes and **(G)** the remaining RNA-seq–identified sex-differentially expressed genes. $ indicates a significant sex difference [$P<0.05$] or a tendency to differ [$P<0.10$, ($)] by unpaired *t* tests. **(B–F** and **H–J)** mRNA expression levels of the indicated genes. Two-way repeated measures ANOVA was performed to identify the effects of sex and progesterone in each RU486 condition. Significant effects are presented as follows: (S), $P_{sex}<0.10$; S, $P_{sex}<0.05$; SS, $P_{sex}<0.01$; SSS, $P_{sex}<0.001$; (P), $P_{progesterone}<0.10$; P, $P_{progesterone}<0.05$; PP, $P_{progesterone}<0.01$; PPP, $P_{progesterone}<0.001$; (×), $P_{sex\times progesterone}<0.10$; ×, $P_{sex\times progesterone}<0.05$; and ××, $P_{sex\times progesterone}<0.01$. Dunnett's *post hoc* tests were applied when appropriate. * indicates a significant difference [$P<0.05$] and (*) indicates a tendency to differ [$P<0.10$] from the EtOH control.

Effects of progesterone on adipocyte markers in SVF-differentiated brown adipocytes

Since our results suggest that progesterone may regulate some of the sex-differentially expressed genes in BAT, we next determined whether progesterone affects adipocyte function by analyzing the expression of common adipocyte markers in differentiated SVFs. At basal conditions, mRNA expression of *Ucp1* and its transcription activator *Ppargc1a* were higher in female adipocytes than in male adipocytes, but both failed to reach significance (P>0.10; **Fig. 4A**). Female adipocytes had significantly higher expression levels of adipogenic differentiation and maturation genes *Pparg*, *Fabp4*, and *Adipoq* than male adipocytes (**Fig. 4A**). In addition, female adipocytes had a lower expression of the classical white adipocyte marker *Lep* than male adipocytes, suggesting a more metabolically active phenotype of female differentiated SVFs from BAT (**Fig. 4A**), although it should be noted that *Lep* mRNA expression was relatively low in these cells. Progesterone treatment did not significantly affect expression levels of *Ucp1* (**Fig. 4B**), *Ppargc1a* (**Fig. 4C**), *Pparg* (**Fig. 4D**), and *Fabp4* (**Fig. 4E**). Intriguingly, progesterone dose-dependently reduced *Adipoq* mRNA expression in adipocytes of both sexes (**Fig. 4F**), of which the inhibitory effect of progesterone was also likely driven by GR since the effect was marginally affected by 5 nM of RU486 cotreatment but was blunted by 500 nM of RU486 cotreatment.

Effects of progesterone in a brown adipocyte cell line

To confirm the effects of progesterone on the expression of common brown adipocyte markers, we stimulated differentiated T37i, a female brown adipocyte cell line, with progesterone for 24 hours. High doses of progesterone significantly reduced *Ucp1* mRNA expression (**Fig. 5A**) but did not significantly influence mRNA expression of *Ppargc1a* (**Fig. 5B**). In contrast, *Pparg* mRNA expression was induced by high doses of progesterone (**Fig. 5C**). Interestingly, mRNA expression of *Fabp4* was induced by 10^{-6} and $10^{-5.5}$ M of progesterone stimulation, but tended to be reduced by 10^{-5} M of progesterone stimulation (**Fig. 5D**). Expression levels of both adipokines *Adipoq* and *Lep* were reduced by high-dose progesterone stimulation (**Fig. 5E** and **5F**).

Concerning the expression of receptors that can potentially mediate the effects of progesterone, we found that *Pgr* mRNA expression could not be detected in the T37i cells (data not shown) while *Nr3c1* mRNA expression was downregulated by progesterone stimulation, albeit only statistically significant at the highest tested concentration of 10^{-5} M (**Fig. 5G**). Transcription levels of the GR target genes *Tsc22d3* (**Fig. 5H**) and *Fkbp5* (data not shown) were dose-dependently upregulated, supporting an effect likely driven by the GR-signaling cascade.

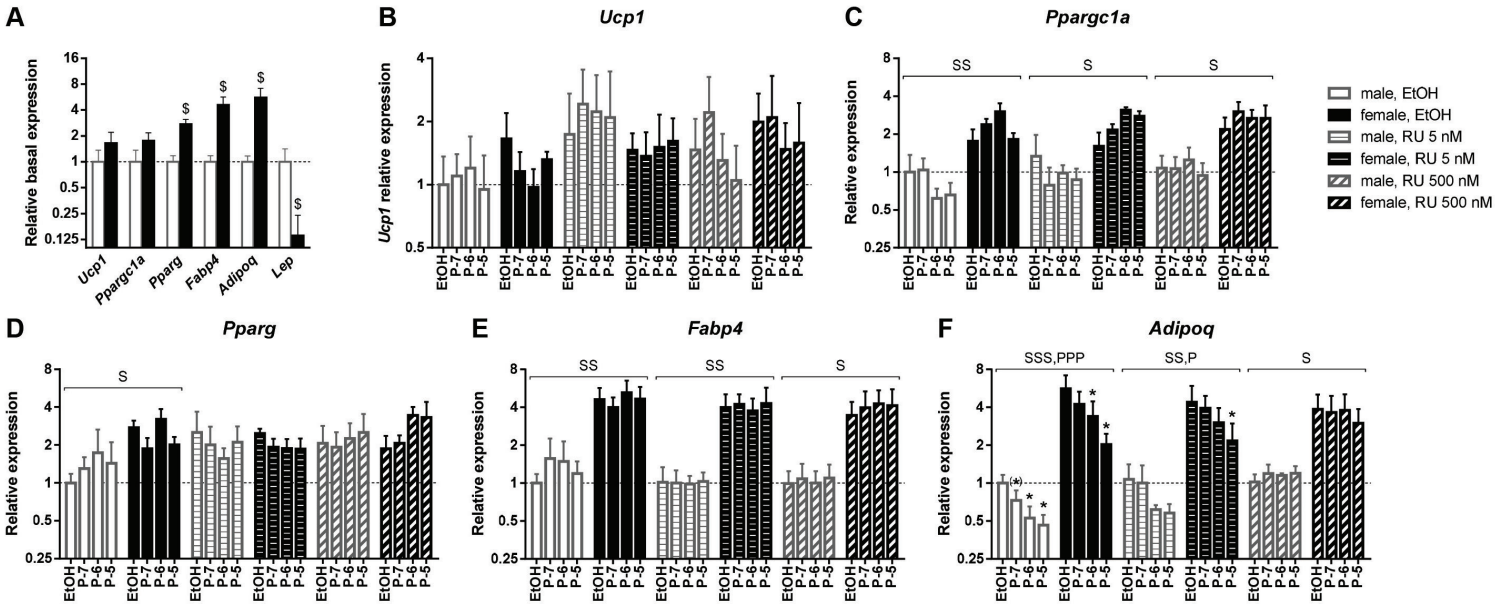

Fig. 4 Effects of progesterone on adipocyte markers in SVF-differentiated brown adipocytes

SVF-derived primary cultures of brown adipocytes from male and female BAT were stimulated with progesterone at indicated concentrations: P-7 (10^{-7} M), P-6 (10^{-6} M), or P-5 (10^{-5} M), together with RU486 (5 or 500 nM) or EtOH vehicle. Expression levels were normalized to *Actb* and *Hprt*, depicted relative to the level of EtOH-treated male adipocytes, and presented as mean±SEM. Data were log-transformed before statistical analyses. **(A)** Basal mRNA expression levels of common adipocyte markers. $ indicates a significant sex difference [P<0.05] by unpaired t tests. **(B–F)** mRNA expression levels of the indicated genes. Two-way repeated measures ANOVA was performed to identify the effects of sex and progesterone in each RU486 condition. Significant effects are presented as follows: S, P_{sex}<0.05; SS, P_{sex}<0.01; SSS, P_{sex}<0.001; P, $P_{progesterone}$<0.05; and PPP, $P_{progesterone}$<0.001. Dunnett's *post hoc* tests were applied when appropriate. * indicates a significant difference [P<0.05] and (*) indicates a tendency to differ [P<0.10] from the EtOH control.

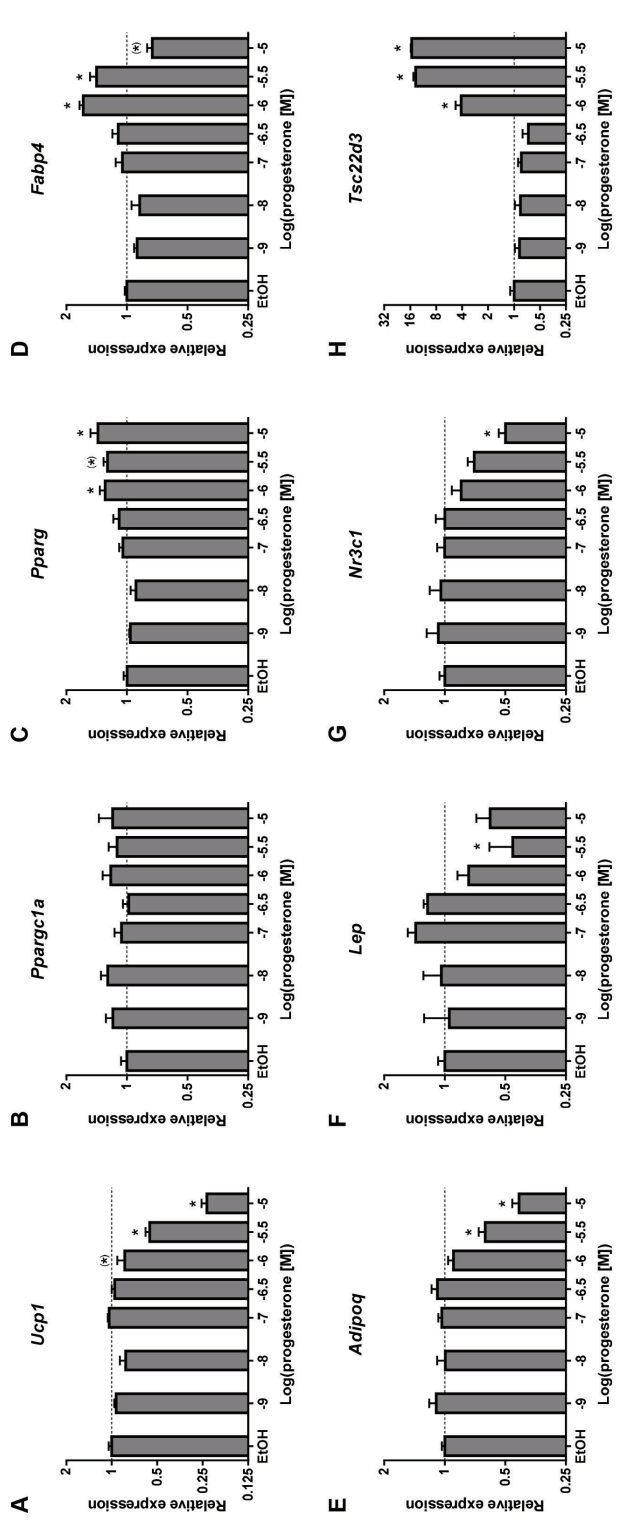

Fig. 5 Effect of progesterone on differentiated T37i brown adipocytes

Differentiated T37i brown adipocytes were treated for 24 hours with progesterone at indicated concentrations. Expression levels were normalized to *Actb* and *B2m*, depicted relative to the EtOH vehicle-treated condition, and presented as mean±SEM. Data were log-transformed before statistical analyses with one-way ANOVA. * indicates a significant difference [$P<0.05$] and (*) indicates a tendency to differ from the EtOH-treated condition by Dunnett's *post hoc* tests.

Since progesterone affected the expression of *Pparg* (the master transcriptional activator of adipogenesis) and *Ucp1* expression in differentiated T37i cells, we next determined the impact of progesterone on T37i differentiation by adding progesterone to the differentiation cocktail. *Ucp1* and *Ppargc1a* (the transcriptional activator of mitochondrial biogenesis) mRNA expression levels were strongly upregulated during differentiation (P_{day}<0.001), but were significantly inhibited in the presence of progesterone at the highest concentration (**Fig. 6A** and **6B**). In contrast, mRNA expression of *Pparg* was induced by co-stimulation with 10^{-6} M and 10^{-5} M of progesterone (**Fig. 6C**), while expression of the mature adipocyte marker *Fabp4* was not significantly regulated by progesterone (**Fig. 6D**). However, at the early differentiation phase (day 3), 10^{-7} M and 10^{-6} M of progesterone induced *Adipoq* mRNA expression, but this effect was absent at later stages when even a downregulation was seen at the highest concentration of 10^{-5} M after 9 days of differentiation (**Fig. 6E**). *Lep* mRNA expression was inhibited at the highest dose of progesterone treatment throughout differentiation (**Fig. 6F**). Of note, mRNA expression levels of a pro-apoptotic marker *Bax* and an anti-apoptotic marker *Bcl2* were not significantly affected by progesterone cotreatment (data not shown), suggesting that progesterone did not hamper cell survival. Subsequently, we tested the NE-induced thermogenic activity in differentiated T37i cells with/without progesterone treatment during differentiation. Cotreatment of high-dose progesterone during differentiation significantly inhibited baseline mRNA expression levels of *Ucp1* (**Fig. 6G**) and *Ppargc1a* (**Fig. 6H**). However, in the presence of progesterone the cells remained responsive to NE since NE stimulation induced the expression of these thermogenic genes in T37i cells, albeit that the NE-induced expression levels were reduced in cells treated with high concentrations of progesterone (**Fig. 6G** and **6H**). Furthermore, NE-induced glycerol release from T37i cells (a measure for thermogenic activity) was dose-dependently reduced by progesterone treatment during adipocyte differentiation (**Fig. 6I**).

Discussion

To the best of our knowledge, this is the first study to investigate sex differences in the global transcriptional profile by RNA-seq in the interscapular BAT of mice at reproductive age and at basal housing conditions. Functional annotation and clustering showed enrichment of genes encoding proteins involved in cellular structure, cell-cell contact, and cell adhesion. Although female BAT was isolated randomly throughout the estrous cycle, the sex-differential expression remained apparent suggesting a robust sex-dependent regulation of transcription in BAT. In support, we confirmed our previous findings by this approach, showing that *Bmp8b* is sex-differentially expressed in BAT (32).

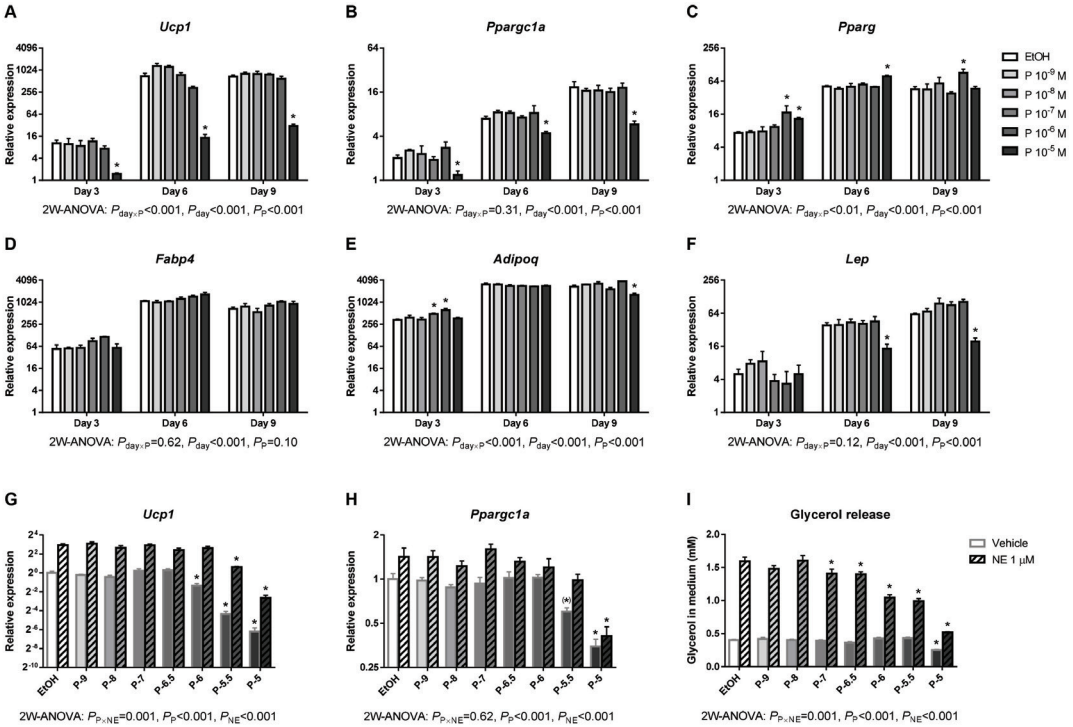

Fig. 6 Effect of progesterone treatment during differentiation of T37i brown adipocytes

Progesterone (P) at indicated concentrations were treated during differentiation of T37i brown preadipocytes until full differentiation at day 9. Data are presented as mean±SEM. Gene expression data were log-transformed before statistical analyses with two-way ANOVA. * indicates a significant difference [P<0.05] and (*) indicates a tendency to differ from the EtOH-treated condition by Dunnett's *post hoc* tests. **(A–F)** Days after differentiation, when the differentiating cells were collected, are plotted on the X axis. Expression levels were normalized with *Actb* and *B2m* and depicted relative to the levels in undifferentiated cells (day 0). **(G–I)** Nine-day differentiated cells with/without progesterone during differentiation were stimulated for 24 hours with 1 μM of norepinephrine (NE) or vehicle and analyzed for mRNA expression or glycerol release in cultured media. Gene expression levels were normalized with *Actb* and *B2m* and depicted relative to levels of the EtOH-treated/vehicle-stimulated condition. Concentrations of progesterone treatment during differentiation are indicated on the X axis as follows: P-9 (10^{-9} M), P-8 (10^{-8} M), P-7 (10^{-7} M), P-6.5 ($10^{-6.5}$ M), P-6 (10^{-6} M), P-5.5 ($10^{-5.5}$ M), and P-5 (10^{-5} M).

Cell adhesion is an essential process in maintaining tissue structure and cellular interaction with neighboring cells or with the extracellular matrix (ECM) (33). Structural and adhesion proteins, such as E-cadherin, claudins, and keratins, are well-known for their role in this process as well as in epithelial-to-mesenchymal transition, cancer progression, and tumor metastasis (34). However, their role in adipose tissues is less clear, although the microenvironment is shown to be important for visceral and subcutaneous WAT morphology and function, including the formation of new vessels to promote optimal tissue expansion (35,36). Upon high-fat diet (HFD) feeding, the murine male gonadal WAT showed a lack of angiogenesis whereas the murine female gonadal WAT had a high vascular density, together with an upregulation of the angiogenic factors, e.g. *Vegfa* and *Vegfr2* (37). The importance of the ECM is also illustrated by a study of Grandl *et al.* (38), showing that adipose progenitor cells isolated from gonadal WAT of male mice differentiated better when they were cultured in decellularized ECM of BAT or subcutaneous WAT than when they were cultured without ECM or in decellularized ECM of visceral WAT (38). In support of our findings in BAT, a study comparing obesity-prone and obesity-resistant rats in response to a HFD showed that genes encoding proteins involved in cell structure and motility constituted almost a quarter of the differentially expressed genes, with the lowest expression in the obesity-prone rats (39). However, no major overlap is observed between the genes detected in that study with our identified genes. Importantly, we observed that the expression of most of the identified structural and cell-adhesion genes was very low in our primary brown adipocyte cultures, despite having detectable expression in BAT itself. This might suggest that *in vivo* these genes are expressed by non-adipocyte cell types in BAT, such as endothelial cells and immune cells, and that these cell types play an essential role in maintaining an optimal microenvironment for BAT (35,40).

Upstream regulator analysis of the sex-differentially expressed genes identified ErbB2 and TGF-β1 as the most significant upstream regulators. ErbB2, a transmembrane tyrosine kinase receptor protein, is present in adipose-derived stem cells and is involved in adipogenic proliferation and differentiation (41). TGF-β1, a member of the TGF-β family of growth and differentiation factors, functions in adipose-derived stem cells to promote angiogenesis for optimal blood supply during adipose expansion (41). In mice, serum TGF-β1 levels correlate with obesity and blocking of its principal signal transducer Smad3 or treatment with a TGF-β neutralizing antibody resulted in browning of WAT and prevented development of obesity (42). Upstream regulator analysis also identified E2, progesterone, and DHT as endogenous hormones regulating the expression of the identified genes. Moreover, the fact that ovariectomy reduced the mRNA expression levels while orchiectomy almost had no significant

effect, strongly suggest a predominant role for female sex steroids in the sex-dimorphic expression pattern in BAT. Analysis of gene expression in primary brown adipocytes, isolated and differentiated from BAT SVF cells of male and female mice, showed that this sex-dependent expression pattern persisted under similar culture conditions. A similar pattern was observed for some of the common brown adipocyte markers, such as *Ppargc1a*, *Pparg*, *Fabp4*, and *Adipoq*. Combined, this suggests that the sex-dependent expression pattern is controlled by sex steroids but also partly by intrinsic factors such as the presence of X- and/or Y-chromosomes as well as epigenetic differences between the sexes. As discussed above, most of the identified structural and cell-adhesion genes are likely expressed by non-adipocytes cell types in BAT. Additional studies are, therefore, needed to determine which cell types express these genes in order to identify their role in BAT and to determine whether these genes are directly regulated by sex steroids. Based on literature, progesterone might be involved in the regulation of the expression of our identified genes, such as *Cdh1*, *Cfd*, and *Lcn2*, since these have been reported to show progesterone-dependent regulation in the endometrium, a tissue that also becomes highly vascularized during the preimplantation stage (43-46).

The role of progesterone in regulating BAT function has been studied in much less detail than the other female sex steroid E2, despite its elevated levels during the luteal phase and pregnancy. Furthermore, available data for progesterone effects on BAT activity are conflicting. Regarding the thermogenic function of BAT, progesterone treatment was found to induce NE-stimulated *Ucp1* mRNA expression in primary cultures of mouse brown adipocytes, but surprisingly only at the lowest stimulatory concentration of 10^{-9} M and not at higher stimulatory concentrations of 10^{-8} or 10^{-7} M (47). The ratio of α_{2A}/β_3-AR receptors in primary brown adipocyte cultures was also reduced by progesterone treatment, reflecting induced thermogenic capacity, by all tested concentrations of 10^{-9}, 10^{-8}, and 10^{-7} M (20). In contrast, another recent study showed that the mRNA expression of *Ucp1* and other thermogenic genes in murine BAT was reduced during pregnancy as well as by *in vivo* progesterone treatment. Furthermore, treatment of primary brown adipocytes by 5×10^{-7} M progesterone reduced NE-stimulated *Ucp1* mRNA expression (48). In our study, progesterone stimulation of primary cultures of brown adipocytes at a physiological concentration for female mice (10^{-7} M) (49) or at supra-physiological concentrations (10^{-6} and 10^{-5} M) did not affect *Ucp1* mRNA expression. However, in the T37i brown adipocyte cell line, progesterone treatment at high concentrations ($10^{-5.5}$ and 10^{-5} M) clearly inhibited *Ucp1* mRNA expression. Expression of common mature brown adipocyte markers such as *Ppargc1a*, *Pparg*, and *Fabp4* was not regulated by progesterone in primary cultures, although they showed a sex-

dependent expression being higher in female than in male adipocytes. Of note, concentrations of progesterone used in our study should be adequate to mediate progesterone effects because its equilibrium dissociation constant (K_d) has been reported to be 2–3 nM in various tissues (50). Further studies are required to investigate *in vivo* effects of progesterone on the BAT transcriptional profile and function to draw firm conclusions about the role of progesterone in the regulation of BAT and its importance for clinically relevant conditions.

Apart from its role in thermogenesis, BAT also serves as an endocrine organ, secreting several proteins including adiponectin and adipsin (also known as complement factor D) (51,52), of which the gene expression in primary brown adipocytes was dose-dependently reduced by progesterone. Adiponectin is a metabolic-favorable adipokine, having insulin-sensitizing and anti-inflammatory effects, of which the plasma concentrations are reduced in obesity (53,54). It has been reported that plasma adiponectin levels and adiponectin protein expressions in BAT and gonadal WAT are higher in female mice than in male mice, but no sex-dependent pattern was observed in mRNA expression levels (55). The fact that ovariectomy increased while pregnancy decreased plasma adiponectin levels suggest an inhibitory effect of progesterone (or other pregnancy-related hormones) on adiponectin secretion from adipocytes (55), which is in line with our *in vitro* results. However, another study in female rats found no significant effect of progesterone treatment on *Adipoq* mRNA expression in BAT but instead observed reduced *Adipoq* mRNA in inguinal WAT (56). Adipsin is necessary for initiation of the alternative complement pathway, an innate immune response for pathogen recognition and elimination (57) and plays a role in maintaining pancreatic β cell function (58). Adipsin also indirectly promotes adipogenesis and triglyceride storage in adipocytes via the product of its enzymatic action, the acylation-stimulating protein (ASP) (59,60). However, adipsin-deficient mice show a normal body weight (57), but reduced tissue inflammation, illustrated by reduced macrophages and crown-like structures in WAT, upon HFD treatment (58). Our results show that progesterone inhibited adipsin expression in primary brown adipocytes of murine origin. It remains to be determined how these results translate to human since serum adipsin levels were reduced during pregnancy but did not differ between the follicular and luteal phase in humans (61).

Studies have shown systemic metabolic effects of another adipokine lipocalin 2 although the findings are conflicting. Compared to lean controls, serum lipocalin 2 levels were higher in mouse models of obesity, such as *ob*/*ob* mice, *db*/*db* mice, and HFD feeding (62). Reduction of *Lcn2* expression in 3T3-L1 adipocytes by short-hairpin RNA resulted in improved insulin sensitivity (62). In contrast, lipocalin 2-deficient male mice were more obese and had more severe diet-induced insulin resistance as well as impaired thermogenic activity in BAT

upon cold exposure, compared to wild-type males (63). Lipocalin 2-deficient females were also more obese than wild-type females upon HFD feeding (64). Although lipocalin 2 was previously reported to be expressed in murine WAT but not in BAT depots (62), we could detect *Lcn2* mRNA expression in BAT depots and differentiated BAT SVFs, in which we found that female mice have a higher *Lcn2* expression which might be attributable to progesterone. More dedicated studies are required in order to draw firm conclusions on the regulation of lipocalin 2 in BAT.

Interestingly, using different concentrations of RU486 revealed that the progesterone-inhibiting effects on mRNA expression of various genes in brown adipocytes are likely driven by GR rather than PR because the inhibition was blunted when RU486 was applied at a GR- and PR- antagonistic concentration but not at a more PR-specific antagonistic concentration (31). Our findings are in agreement with previous studies, for instance, progesterone was reported to act via the GR to mediate regulatory T cells enrichment (65) and to repress *PTGS2* mRNA expression in myometrial cells (66). However, non-genomic actions of progesterone, e.g. through progesterone membrane receptors and the progesterone receptor membrane components, cannot be ruled out.

In summary, this study demonstrates a sex-dependent transcriptomic profile in BAT of mice at basal conditions and suggests a role for progesterone in the expression pattern of some of the identified sex differentially expressed genes. Furthermore, our results highlight a role for genes encoding proteins involved in cellular structure, cell-cell contact, and cell adhesion in the sex-differential function of BAT.

Acknowledgements

We would like to thank Chen Hu for her valuable assistance during the experiment.

Additional Information

Disclosure Summary

The authors have nothing to disclose.

Data availability

RNA-seq FASTQ files are available at ArrayExpress database of the EMBL's European Bioinformatics Institute (accession no. E-MTAB-8717). An Excel file summarizing the enrichment and pathway analyses in DAVID and IPA is available upon request to the corresponding author.

References and Notes

1. GBD 2015 Obesity Collaborators, Afshin A, Forouzanfar MH, Reitsma MB, Sur P, Estep K, Lee A, et al. Health Effects of Overweight and Obesity in 195 Countries over 25 Years. *N Engl J Med*. 2017;**377**(1):13-27.
2. Logue J, Walker JJ, Colhoun HM, Leese GP, Lindsay RS, McKnight JA, Morris AD, et al. Do men develop type 2 diabetes at lower body mass indices than women? *Diabetologia*. 2011;**54**(12):3003-3006.
3. Longo M, Zatterale F, Naderi J, Parrillo L, Formisano P, Raciti GA, Beguinot F, Miele C. Adipose Tissue Dysfunction as Determinant of Obesity-Associated Metabolic Complications. *International journal of molecular sciences*. 2019;**20**(9).
4. Palmer BF, Clegg DJ. The sexual dimorphism of obesity. *Mol Cell Endocrinol*. 2015;**402**:113-119.
5. Townsend K, Tseng YH. Brown adipose tissue: Recent insights into development, metabolic function and therapeutic potential. *Adipocyte*. 2012;**1**(1):13-24.
6. Cannon B, Nedergaard J. Brown adipose tissue: function and physiological significance. *Physiol Rev*. 2004;**84**(1):277-359.
7. Feldmann HM, Golozoubova V, Cannon B, Nedergaard J. UCP1 ablation induces obesity and abolishes diet-induced thermogenesis in mice exempt from thermal stress by living at thermoneutrality. *Cell Metab*. 2009;**9**(2):203-209.
8. Moonen MPB, Nascimento EBM, van Marken Lichtenbelt WD. Human brown adipose tissue: Underestimated target in metabolic disease? *Biochim Biophys Acta Mol Cell Biol Lipids*. 2019;**1864**(1):104-112.
9. Newell-Fugate AE. The role of sex steroids in white adipose tissue adipocyte function. *Reproduction*. 2017;**153**(4):R133-R149.
10. Mauvais-Jarvis F. Sex differences in metabolic homeostasis, diabetes, and obesity. *Biol Sex Differ*. 2015;**6**:14.
11. Cypess AM, Lehman S, Williams G, Tal I, Rodman D, Goldfine AB, Kuo FC, et al. Identification and importance of brown adipose tissue in adult humans. *N Engl J Med*. 2009;**360**(15):1509-1517.
12. Rodriguez-Cuenca S, Pujol E, Justo R, Frontera M, Oliver J, Gianotti M, Roca P. Sex-dependent thermogenesis, differences in mitochondrial morphology and function, and adrenergic response in brown adipose tissue. *J Biol Chem*. 2002;**277**(45):42958-42963.
13. Geer EB, Shen W. Gender differences in insulin resistance, body composition, and energy balance. *Gend Med*. 2009;**6 Suppl 1**:60-75.
14. Mauvais-Jarvis F, Clegg DJ, Hevener AL. The role of estrogens in control of energy balance and glucose homeostasis. *Endocr Rev*. 2013;**34**(3):309-338.
15. Gonzalez-Garcia I, Tena-Sempere M, Lopez M. Estradiol Regulation of Brown Adipose Tissue Thermogenesis. *Adv Exp Med Biol*. 2017;**1043**:315-335.
16. Yoshioka K, Yoshida T, Wakabayashi Y, Nishioka H, Kondo M. Reduced brown adipose tissue thermogenesis of obese rats after ovariectomy. *Endocrinol Jpn*. 1988;**35**(4):537-543.
17. Rogers NH, Perfield JW, 2nd, Strissel KJ, Obin MS, Greenberg AS. Reduced energy expenditure and increased inflammation are early events in the development of ovariectomy-induced obesity. *Endocrinology*. 2009;**150**(5):2161-2168.
18. Martinez de Morentin PB, Gonzalez-Garcia I, Martins L, Lage R, Fernandez-Mallo D, Martinez-Sanchez N, Ruiz-Pino F, et al. Estradiol regulates brown adipose tissue thermogenesis via hypothalamic AMPK. *Cell Metab*. 2014;**20**(1):41-53.
19. Hashimoto O, Noda T, Morita A, Morita M, Ohtsuki H, Sugiyama M, Funaba M. Castration induced browning in subcutaneous white adipose tissue in male mice. *Biochem Biophys Res Commun*. 2016;**478**(4):1746-1750.
20. Monjo M, Rodriguez AM, Palou A, Roca P. Direct effects of testosterone, 17 beta-estradiol, and progesterone on adrenergic regulation in cultured brown adipocytes: potential mechanism for gender-dependent thermogenesis. *Endocrinology*. 2003;**144**(11):4923-4930.
21. Kaikaew K, Steenbergen J, Themmen APN, Visser JA, Grefhorst A. Sex difference in thermal preference of adult mice does not depend on presence of the gonads. *Biol Sex Differ*. 2017;**8**(1):24.
22. Martin M. Cutadapt removes adapter sequences from high-throughput sequencing reads. *EMBnet.journal*. 2011;**17**(1):3.
23. Dobin A, Davis CA, Schlesinger F, Drenkow J, Zaleski C, Jha S, Batut P, Chaisson M, Gingeras TR. STAR: ultrafast universal RNA-seq aligner. *Bioinformatics*. 2013;**29**(1):15-21.

24. Liao Y, Smyth GK, Shi W. featureCounts: an efficient general purpose program for assigning sequence reads to genomic features. *Bioinformatics*. 2014;**30**(7):923-930.
25. Love MI, Huber W, Anders S. Moderated estimation of fold change and dispersion for RNA-seq data with DESeq2. *Genome Biol*. 2014;**15**(12):550.
26. Huang da W, Sherman BT, Lempicki RA. Systematic and integrative analysis of large gene lists using DAVID bioinformatics resources. *Nat Protoc*. 2009;**4**(1):44-57.
27. Kramer A, Green J, Pollard J, Jr., Tugendreich S. Causal analysis approaches in Ingenuity Pathway Analysis. *Bioinformatics*. 2014;**30**(4):523-530.
28. RRID:CVCL_S893. https://scicrunch.org/resolver/CVCL_S893.
29. Kaikaew K, Steenbergen J, van Dijk TH, Grefhorst A, Visser JA. Sex Difference in Corticosterone-Induced Insulin Resistance in Mice. *Endocrinology*. 2019;**160**(10):2367-2387.
30. Kaikaew K, Grefhorst A, Steenbergen J, Swagemakers SMA, McLuskey A, Visser JA. Sex difference in the mouse BAT transcriptome reveals a role of progesterone in BAT function: Supplementary data. Mendeley Data 2020. Deposited 15 January 2020. https://data.mendeley.com/datasets/t3jc3k7dct/1.
31. Kroon J, Koorneef LL, van den Heuvel JK, Verzijl CRC, van de Velde NM, Mol IM, Sips HCM, Hunt H, Rensen PCN, Meijer OC. Selective Glucocorticoid Receptor Antagonist CORT125281 Activates Brown Adipose Tissue and Alters Lipid Distribution in Male Mice. *Endocrinology*. 2018;**159**(1):535-546.
32. Grefhorst A, van den Beukel JC, van Houten EL, Steenbergen J, Visser JA, Themmen AP. Estrogens increase expression of bone morphogenetic protein 8b in brown adipose tissue of mice. *Biol Sex Differ*. 2015;**6**:7.
33. Gumbiner BM. Cell adhesion: the molecular basis of tissue architecture and morphogenesis. *Cell*. 1996;**84**(3):345-357.
34. Basu S, Cheriyamundath S, Ben-Ze'ev A. Cell-cell adhesion: linking Wnt/beta-catenin signaling with partial EMT and stemness traits in tumorigenesis. *F1000Res*. 2018;**7**.
35. Pope BD, Warren CR, Parker KK, Cowan CA. Microenvironmental Control of Adipocyte Fate and Function. *Trends Cell Biol*. 2016;**26**(10):745-755.
36. Choe SS, Huh JY, Hwang IJ, Kim JI, Kim JB. Adipose Tissue Remodeling: Its Role in Energy Metabolism and Metabolic Disorders. *Front Endocrinol (Lausanne)*. 2016;**7**:30.
37. Rudnicki M, Abdifarkosh G, Rezvan O, Nwadozi E, Roudier E, Haas TL. Female Mice Have Higher Angiogenesis in Perigonadal Adipose Tissue Than Males in Response to High-Fat Diet. *Front Physiol*. 2018;**9**:1452.
38. Grandl G, Muller S, Moest H, Moser C, Wollscheid B, Wolfrum C. Depot specific differences in the adipogenic potential of precursors are mediated by collagenous extracellular matrix and Flotillin 2 dependent signaling. *Mol Metab*. 2016;**5**(10):937-947.
39. Joo JI, Yun JW. Gene expression profiling of adipose tissues in obesity susceptible and resistant rats under a high fat diet. *Cell Physiol Biochem*. 2011;**27**(3-4):327-340.
40. Panina YA, Yakimov AS, Komleva YK, Morgun AV, Lopatina OL, Malinovskaya NA, Shuvaev AN, Salmin VV, Taranushenko TE, Salmina AB. Plasticity of Adipose Tissue-Derived Stem Cells and Regulation of Angiogenesis. *Front Physiol*. 2018;**9**:1656.
41. Scioli MG, Bielli A, Gentile P, Mazzaglia D, Cervelli V, Orlandi A. The biomolecular basis of adipogenic differentiation of adipose-derived stem cells. *International journal of molecular sciences*. 2014;**15**(4):6517-6526.
42. Yadav H, Quijano C, Kamaraju AK, Gavrilova O, Malek R, Chen W, Zerfas P, et al. Protection from obesity and diabetes by blockade of TGF-beta/Smad3 signaling. *Cell Metab*. 2011;**14**(1):67-79.
43. Jha RK, Titus S, Saxena D, Kumar PG, Laloraya M. Profiling of E-cadherin, beta-catenin and Ca(2+) in embryo-uterine interactions at implantation. *FEBS Lett*. 2006;**580**(24):5653-5660.
44. Jeong JW, Lee KY, Kwak I, White LD, Hilsenbeck SG, Lydon JP, DeMayo FJ. Identification of murine uterine genes regulated in a ligand-dependent manner by the progesterone receptor. *Endocrinology*. 2005;**146**(8):3490-3505.
45. Yao MW, Lim H, Schust DJ, Choe SE, Farago A, Ding Y, Michaud S, Church GM, Maas RL. Gene expression profiling reveals progesterone-mediated cell cycle and immunoregulatory roles of Hoxa-10 in the preimplantation uterus. *Mol Endocrinol*. 2003;**17**(4):610-627.
46. Liu YF, Deng WB, Li SY, Yao MN, Liu J, Dou HT, Zhao ML, Yang ZM, Liang XH. Progesterone induces the expression of lipocalin-2 through Akt-c-Myc pathway during mouse decidualization. *FEBS Lett*. 2016;**590**(16):2594-2602.

47. Rodriguez AM, Monjo M, Roca P, Palou A. Opposite actions of testosterone and progesterone on UCP1 mRNA expression in cultured brown adipocytes. *Cell Mol Life Sci.* 2002;**59**(10):1714-1723.
48. McIlvride S, Mushtaq A, Papacleovoulou G, Hurling C, Steel J, Jansen E, Abu-Hayyeh S, Williamson C. A progesterone-brown fat axis is involved in regulating fetal growth. *Sci Rep.* 2017;**7**(1):10671.
49. Nilsson ME, Vandenput L, Tivesten A, Norlen AK, Lagerquist MK, Windahl SH, Borjesson AE, et al. Measurement of a Comprehensive Sex Steroid Profile in Rodent Serum by High-Sensitive Gas Chromatography-Tandem Mass Spectrometry. *Endocrinology.* 2015;**156**(7):2492-2502.
50. Jacobs BR, Smith RG. A comparison of progesterone and R5020 binding in endometrium, ovary, pituitary, and hypothalamus. *Fertil Steril.* 1981;**35**(4):438-441.
51. Ali Khan A, Hansson J, Weber P, Foehr S, Krijgsveld J, Herzig S, Scheideler M. Comparative Secretome Analyses of Primary Murine White and Brown Adipocytes Reveal Novel Adipokines. *Mol Cell Proteomics.* 2018;**17**(12):2358-2370.
52. Villarroya J, Cereijo R, Gavalda-Navarro A, Peyrou M, Giralt M, Villarroya F. New insights into the secretory functions of brown adipose tissue. *J Endocrinol.* 2019.
53. Stern JH, Rutkowski JM, Scherer PE. Adiponectin, Leptin, and Fatty Acids in the Maintenance of Metabolic Homeostasis through Adipose Tissue Crosstalk. *Cell Metab.* 2016;**23**(5):770-784.
54. Achari AE, Jain SK. Adiponectin, a Therapeutic Target for Obesity, Diabetes, and Endothelial Dysfunction. *International journal of molecular sciences.* 2017;**18**(6):E1321.
55. Combs TP, Berg AH, Rajala MW, Klebanov S, Iyengar P, Jimenez-Chillaron JC, Patti ME, Klein SL, Weinstein RS, Scherer PE. Sexual differentiation, pregnancy, calorie restriction, and aging affect the adipocyte-specific secretory protein adiponectin. *Diabetes.* 2003;**52**(2):268-276.
56. Stelmanska E, Kmiec Z, Swierczynski J. The gender- and fat depot-specific regulation of leptin, resistin and adiponectin genes expression by progesterone in rat. *J Steroid Biochem Mol Biol.* 2012;**132**(1-2):160-167.
57. Xu Y, Ma M, Ippolito GC, Schroeder HW, Jr., Carroll MC, Volanakis JE. Complement activation in factor D-deficient mice. *Proc Natl Acad Sci U S A.* 2001;**98**(25):14577-14582.
58. Lo JC, Ljubicic S, Leibiger B, Kern M, Leibiger IB, Moede T, Kelly ME, et al. Adipsin is an adipokine that improves beta cell function in diabetes. *Cell.* 2014;**158**(1):41-53.
59. Cianflone K, Xia Z, Chen LY. Critical review of acylation-stimulating protein physiology in humans and rodents. *Biochim Biophys Acta.* 2003;**1609**(2):127-143.
60. Song NJ, Kim S, Jang BH, Chang SH, Yun UJ, Park KM, Waki H, Li DY, Tontonoz P, Park KW. Small Molecule-Induced Complement Factor D (Adipsin) Promotes Lipid Accumulation and Adipocyte Differentiation. *PLoS One.* 2016;**11**(9):e0162228.
61. Poveda NE, Garces MF, Ruiz-Linares CE, Varon D, Valderrama S, Sanchez E, Castiblanco-Cortes A, et al. Serum Adipsin Levels throughout Normal Pregnancy and Preeclampsia. *Sci Rep.* 2016;**6**:20073.
62. Yan QW, Yang Q, Mody N, Graham TE, Hsu CH, Xu Z, Houstis NE, Kahn BB, Rosen ED. The adipokine lipocalin 2 is regulated by obesity and promotes insulin resistance. *Diabetes.* 2007;**56**(10):2533-2540.
63. Guo H, Jin D, Zhang Y, Wright W, Bazuine M, Brockman DA, Bernlohr DA, Chen X. Lipocalin-2 deficiency impairs thermogenesis and potentiates diet-induced insulin resistance in mice. *Diabetes.* 2010;**59**(6):1376-1385.
64. Guo H, Zhang Y, Brockman DA, Hahn W, Bernlohr DA, Chen X. Lipocalin 2 deficiency alters estradiol production and estrogen receptor signaling in female mice. *Endocrinology.* 2012;**153**(3):1183-1193.
65. Engler JB, Kursawe N, Solano ME, Patas K, Wehrmann S, Heckmann N, Luhder F, et al. Glucocorticoid receptor in T cells mediates protection from autoimmunity in pregnancy. *Proc Natl Acad Sci U S A.* 2017;**114**(2):E181-E190.
66. Lei K, Chen L, Georgiou EX, Sooranna SR, Khanjani S, Brosens JJ, Bennett PR, Johnson MR. Progesterone acts via the nuclear glucocorticoid receptor to suppress IL-1beta-induced COX-2 expression in human term myometrial cells. *PLoS One.* 2012;**7**(11):e50167.

Supplementary table Selected genes from the significant functional annotation clusters and their functional description

Gene	Full name	Description and biological function
Bmp8b	Bone morphogenetic protein 8b	This gene encodes a secreted ligand of the transforming growth factor (TGF)-β superfamily. These ligands bind various TGF-β receptors leading to recruitment and activation of SMAD family transcription factors that regulate gene expression. BMP8b may play a role in the generation of primordial germ cells and has been shown to stimulate thermogenesis in brown adipose tissue. Homozygous knockout mice of both sexes exhibit impaired thermogenesis and reduced metabolic rate, resulting in weight gain.
C7*	Complement component 7	This gene encodes a serum glycoprotein that forms a membrane attack complex together with complement components C5b, C6, C8, and C9 as part of the terminal complement pathway of the innate immune system. The protein encoded by this gene contains a cholesterol-dependent cytolysin/membrane attack complex/perforin-like (CDC/MACPF) domain and belongs to a large family of structurally related molecules that form pores involved in host immunity and bacterial pathogenesis. This protein initiates membrane attack complex formation by binding to the C5b-C6 subcomplex and inserts into the phospholipid bilayer, serving as a membrane anchor.
Cdh1	Cadherin 1	This gene encodes E-cadherin, a calcium-dependent cell adhesion molecule that functions in the establishment and maintenance of epithelial cell morphology.
Cfd	Complement factor D (adipsin)	This gene encodes a serine protease that plays an important role in the alternative pathway of complement activation for pathogen recognition and elimination. The encoded preproprotein undergoes proteolytic processing to generate a mature, functional enzyme that in turn cleaves factor B in the complement pathway. This gene is expressed in adipocytes and the mature enzyme is secreted into the bloodstream. Mice lacking the encoded product cannot initiate the alternative pathway of complement activation.
Cldn3	Claudin 3	This gene encodes a member of the claudin family. Claudins are integral membrane proteins and components of tight junction strands. Tight junction strands serve as a physical barrier to prevent solutes and water from passing freely through the paracellular space between epithelial or endothelial cell sheets, and also play critical roles in maintaining cell polarity and signal transductions. CLDN3 is predominantly present in brain endothelial cells, where it plays a specific role in the establishment and maintenance of blood-brain barrier tight junction morphology.
Cldn4	Claudin 4	In addition to the general claudin family properties, CLDN4 augments alveolar epithelial barrier function and is induced in acute lung injury.
Cldn7	Claudin 7	In addition to the general claudin family properties, CLDN7 is expressed constitutively in the mammary epithelium throughout development and might be involved in vesicle trafficking to the basolateral membrane. CLDN7 is essential for NaCl homeostasis in distal nephrons.
Cxcl13*	Chemokine (C-X-C motif) ligand 13	CXCL13 is a B lymphocyte chemoattractant strongly expressed in the follicles of the spleen, lymph nodes, and Peyer's patches. It preferentially promotes the migration of B lymphocytes (compared to T cells and macrophages), apparently by stimulating calcium influx into, and chemotaxis of, cells expressing Burkitt's lymphoma receptor 1 (BLR-1).
Epcam*	Epithelial cell adhesion molecule	This gene encodes a carcinoma-associated antigen and is a member of a family that includes at least two type I membrane proteins. This antigen is expressed on most normal epithelial cells and gastrointestinal carcinomas and functions as a homotypic calcium-independent cell adhesion molecule.

Gene	Full name	Description and biological function
Irf4*	Interferon regulatory factor 4	This gene encodes a protein belonging to the IRF (interferon regulatory factor) family of transcription factors, characterized by a unique tryptophan pentad repeat DNA-binding domain. The IRFs are important in the regulation of interferons in response to infection by virus, and in the regulation of interferon-inducible genes. This family member negatively regulates Toll-like-receptor (TLR) signaling that is central to the activation of innate and adaptive immune systems.
Krt5*	Keratin 5	This gene encodes a member of the keratin gene family. The type II cytokeratins consist of basic or neutral proteins which are arranged in pairs of heterotypic keratin chains coexpressed during differentiation of simple and stratified epithelial tissues. KRT5 is specifically expressed in the basal layer of the epidermis with family member KRT14.
Krt8*	Keratin 8	This gene is a member of the type II keratin family. Type I and type II keratins heteropolymerize to form intermediate-sized filaments in the cytoplasm of epithelial cells. The product of this gene typically dimerizes with KRT18 to form an intermediate filament in simple single-layered epithelial cells. This protein plays a role in maintaining cellular structural integrity and also functions in signal transduction and cellular differentiation.
Krt14	Keratin 14	This gene encodes a member of the keratin family, the most diverse group of intermediate filaments. This gene product, a type I keratin, is usually found as a heterotetramer with two KRT5 molecules, a type II keratin. Together they form the cytoskeleton of epithelial cells.
Krt18*	Keratin 18	This gene encodes the type I intermediate filament chain keratin 18. KRT18 and its filament partner KRT8 are perhaps the most commonly found members of the intermediate filament gene family. They are expressed in single layer epithelial tissues of the body.
Lcn2*	Lipocalin 2	This gene encodes a protein that belongs to the lipocalin family. Members of this family transport small hydrophobic molecules such as lipids, steroid hormones and retinoids. The protein encoded by this gene is a neutrophil gelatinase-associated lipocalin and plays a role in innate immunity by limiting bacterial growth as a result of sequestering iron-containing siderophores. The presence of this protein in blood and urine is an early biomarker of acute kidney injury. This protein is thought to be involved in multiple cellular processes, including maintenance of skin homeostasis, and suppression of invasiveness and metastasis. Mice lacking this gene are more susceptible to bacterial infection than wild type mice.
Mup22#	Major urinary protein 22	Major urinary proteins (MUPs) are members of the lipocalin family, which shares almost 99% sequence identity. Unlike lipocalin genes that are expressed in both humans and mice, MUP genes are only expressed in mice. MUPs are mainly expressed in the liver, secreted to the bloodstream, and excreted by the kidney. MUPs are involved in the communication in urine-derived scent marks and can also serve as pheromones. Circulating MUPs may also contribute to regulation of nutrient metabolism, possibly by suppressing hepatic gluconeogenesis and lipid metabolism. However, it remains unclear how MUPs regulate energy metabolism.
Pgr	Progesterone receptor	This gene encodes a member of the steroid receptor superfamily. The encoded protein mediates the physiological effects of progesterone, which plays a central role in reproductive events associated with the establishment and maintenance of pregnancy.
Ptprf*	Protein tyrosine phosphatase receptor type F	This gene encodes a protein in the protein tyrosine phosphatase (PTP) family. PTPs are known to be signaling molecules that regulate a variety of cellular processes including cell growth, differentiation, mitotic cycle, and oncogenic transformation. This PTP possesses an extracellular region, a single transmembrane region, and two tandem intracytoplasmic catalytic domains, and thus represents a receptor-type PTP. The extracellular region contains three Ig-like domains, and nine non-Ig like domains similar to that of neural-cell adhesion molecule. This PTP was shown to function in the regulation of epithelial cell-cell contacts at adherents junctions, as well as in the control of beta-catenin signaling.

Gene	Full name	Description and biological function
Scnn1b*	Sodium channel epithelial 1 beta subunit	Nonvoltage-gated, amiloride-sensitive, sodium channels control fluid and electrolyte transport across epithelia in many organs. These channels are heteromeric complexes consisting of 3 subunits: alpha, beta, and gamma. This gene encodes the beta subunit, and mutations in this gene have been associated with pseudohypoaldosteronism type 1 (PHA1), and Liddle syndrome.
Sdc1*	Syndecan 1	This gene encodes a transmembrane (type I) heparan sulfate proteoglycan which is a member of the syndecan proteoglycan family. The syndecans mediate cell binding, cell signaling, and cytoskeletal organization and syndecan receptors are required for internalization of the HIV-1 tat protein. The syndecan-1 protein functions as an integral membrane protein and participates in cell proliferation, cell migration and cell-matrix interactions via its receptor for extracellular matrix proteins.
St14*	Suppression of tumorigenicity 14	This gene encodes an epithelial-derived, integral membrane serine protease. This protease forms a complex with the Kunitz-type serine protease inhibitor, HAI-1, and is found to be activated by sphingosine 1-phosphate. This protease has been shown to cleave and activate hepatocyte growth factor/scattering factor, and urokinase plasminogen activator, which suggests the function of this protease as an epithelial membrane activator for other proteases and latent growth factors.
Wfdc2*	WAP four-disulfide core domain 2	This gene encodes a protein that is a member of the WFDC domain family. The WFDC domain, or WAP Signature motif, contains eight cysteines forming four disulfide bonds at the core of the protein, and functions as a protease inhibitor in many family members. This gene is expressed in pulmonary epithelial cells. The encoded protein is a small secretory protein, which may be involved in sperm maturation.

Functional description was extracted from NCBI gene database (https://www.ncbi.nlm.nih.gov/gene).

* The mouse-specific description summary was not available and was obtained from its human ortholog.

Information was based on general function of the MUP family, obtained from Charkoftaki G, Wang Y, McAndrews M, Bruford EA, Thompson DC, Vasiliou V, Nebert DW. Update on the human and mouse lipocalin (LCN) gene family, including evidence the mouse Mup cluster is the result of an "evolutionary bloom". *Hum Genomics*. 2019;**13**(1):11.